We are IntechOpen, the world's leading publisher of Open Access books Built by scientists, for scientists

6,900
Open access books available

185,000
International authors and editors

200M
Downloads

Our authors are among the

154
Countries delivered to

TOP 1%
most cited scientists

12.2%
Contributors from top 500 universities



WEB OF SCIENCE™

Selection of our books indexed in the Book Citation Index in Web of Science™ Core Collection (BKCI)

Interested in publishing with us?
Contact book.department@intechopen.com

Numbers displayed above are based on latest data collected.
For more information visit www.intechopen.com



Chapter 8

The Slow Coastal-Trapped Waves off Subei Bank in the Yellow Sea and Their Climatic Change in the Past Decades

X. San Liang

Additional information is available at the end of the chapter

http://dx.doi.org/10.5772/intechopen.80017

Abstract

Coastal-trapped waves (CTWs) are a class of subinertial signals in the weather frequency band that play a pivotal role in coastal air-sea interaction. However, this important topic seems to be missing in the heated debate in recent years on coastal environmental change and protection. In this chapter, a brief but self-contained introduction of the CTW theory is presented, in the hope of providing a reference for investigators in the relevant fields. Also presented is a numerical scheme for computing the wave properties. As a demonstration, we have conducted a preliminary study of the CTWs for a section across the Subei Bank in the Yellow Sea. By the results, all the computed slow modes, including a bottom-intensified one, seem to be slowing down since two decades ago. They have particularly slowed down in the event when a strong El Niño is followed by a strong La Niña, such as in the 97–98 and 09–10 El Niño events.

Keywords: coastal-trapped wave, Yellow Sea, Jiangsu coast, climate change, ENSO

1. Introduction

Coastal-trapped waves (CTWs) are a class of subinertial waves within the weather frequency band, which have elegant mathematical formulation; in the Northern Hemisphere, they propagate unidirectionally such that the coast lies on the right. In coastal hazard study, the role of CTWs is rarely touched, though its importance in exchanging mass and energy has been well recognized (e.g., [1]). For example, the wind-driven variabilities over the continental margin can be largely explained in terms of CTW properties. These waves play a key role in coastal oceans' response to atmospheric weather changes; they make a major mechanism in the coastal ocean that spreads the atmospheric energy in the alongshore direction, leading to the formation of the

IntechOpen

© 2018 The Author(s). Licensee IntechOpen. Distributed under the terms of the Creative Commons Attribution-NonCommercial 4.0 License (https://creativecommons.org/licenses/by-nc/4.0/), which permits use, distribution and reproduction for non-commercial purposes, provided the original is properly cited.

BY-NC

remotely driven upwelling, and hence regulating coastal processes from far away. Historically, the low-frequency CTW wave motions were first identified along the East Australian coast [2], and soon studied in terms of continental shelf waves (CSW) by Robinson [3], reflecting the early effort in this field at Harvard University ([4], cf. [5]). Systematic CTW studies began with Allen [6], Wang and Mooers [7], Clarke [8], Huthnance [9], to name several. A comprehensive review is referred to Brink [10].

The East China Sea (ECS), including the Yellow Sea (YS), is one of the major marginal seas in the Northwestern Pacific. Despite its long coastline, CTWs are rarely investigated for this region. It seems that most of the CTW studies are in 80s to early 90s, though recently there is a renewed interest with the aid of Hilbert-Huang transform [11]. For example, Feng [12] examined the dissipative trapped waves on a broad shelf; Liu and Qin [13] investigated the

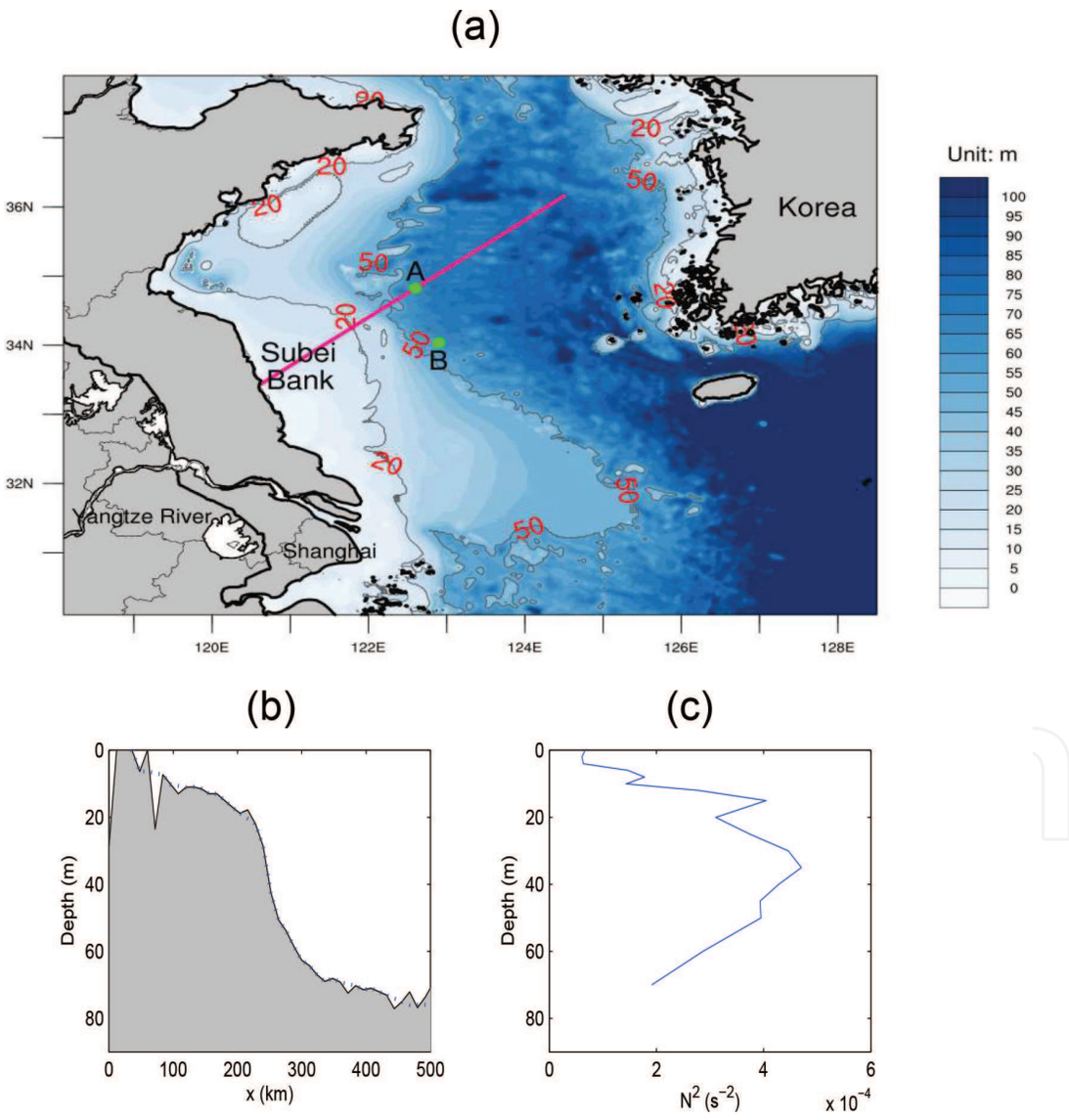


Figure 1. (a) Bathymetry of the Yellow Sea. Abutted to the left is China, while on its right lies Korea. The solid line across Subei Bank marks the cross-section which we will study. Also marked are the points A and B where time series will be extracted from the HYbrid Coordinate Ocean Model (HYCOM) dataset for analysis. (b) The topography along the section marked in (a). (c) A profile of the buoyancy frequency squared N^2 (for 1995).

http://dx.doi.org/10.5772/intechopen.80017

instability of CTWs; Kong et al. [14] studied the impact of the ECS CTWs on Kuroshio; and Chen and Su [15] gave a systematic investigation of continental shelf waves (CSW) along the East China coast. This is in contrast to the South China Sea (SCS), which has attracted much more interest for CTW research; a recent study is referred to Zheng et al. [16].

As the northern part of the ECS, the YS is even less studied in the light of CTWs. This is because the YS is a nearly closed basin with a broad, shallow double shelf, a deep trough lying in between (**Figure 1**). Strictly speaking, CTWs in the traditional sense may not be significant, and, indeed, the YS wave motion is dominated by tides. But previous studies did confirm the existence of CTWs in the YS. Particularly, Chen and Su [15] found they have frequencies around 0.21–0.32 cycle per day (cpd), and a speed of roughly 15 m/s; Wang et al. [17] identified two free CTWs, with phase speeds of 14–19 m/s. A careful and detailed study of the YS CTW was conducted by Hsueh and his group (cf. Hsueh and Pang [18]); it is particularly for the wave motion along the Korea coast.

So far there is almost no study on the CTWs along the Jiangsu coast (particularly off Subei Bank) in the YS. This may be due to the lack of a deep ocean to its east. But, if we focus on some motions local enough, it is conceivable that the trapping condition, that is, vanishing far field, that admits the CTWs may still hold. Besides, such subinertial signals do have been identified (e.g., [15, 17]). Considering the potential importance of CTWs on the processes off Subei Bank, we henceforth conduct a preliminary study for this region. To fit for the scope of this book, we focus on the slow CTW modes and examine their climatic variabilities (see below). On the other hand, we take this opportunity to present a brief but self-contained introduction of the CTW theory, in order to provide environmentalists a reference for this important topic, which is yet to be explored in coastal hazard research.

2. A brief introduction of the coastal-trapped wave theory

2.1. Governing equations

Take a right-hand coordinate system (x, y, z) with x directing offshore and z upward. With the assumption of hydrostaticity and incompressibility, the linearized Boussinesq equations for the free-wave problem on an f-plane in the absence of a basic flow are

$$u_t - fv = -\frac{1}{\rho_0}P_x + \frac{1}{\rho_0}\tau_z^x \tag{1}$$

$$v_t + fu = -\frac{1}{\rho_0}P_y + \frac{1}{\rho_0}\tau_z^y \tag{2}$$

$$\rho = -\frac{1}{g}P_z \tag{3}$$

$$u_x + v_y + w_z = 0 \tag{4}$$

$$\rho_t - \frac{\rho_0}{g}N^2 w = 0 \tag{5}$$

where (u, v, w), ρ, and P are the perturbation velocity, density, and pressure, respectively. The turbulent stress (τ^x, τ^y) will be needed when bottom drag and wind forcing are applied; otherwise, it is usually neglected in the ocean interior. Here, the density field is decomposed into three parts: $\rho_0 + \overline{\rho}(z) + \rho(x, y, z, t)$ with the perturbation field $\rho \ll \overline{\rho} \ll \rho_0$. ρ_0 (usually taken as 1000 or 1025 km/m^3) and g = 9.8 m/s^2 are constants, and $N^2 = -\frac{g}{\rho_0}\frac{\partial \overline{\rho}}{\partial z}$ is the Brunt-Väisälä or buoyancy frequency; $N^2 = N^2(z)$ is given. Suppose that the bottom depth has a dependence on x only, $h = h(x)$, as schematized in **Figure 2**. The boundary conditions are that the perturbation vanishes as $x \to +\infty$, and that no flux crosses the solid boundary. The former is the very costally trapped condition. In the figure, the location $x = b$ is pretended to be where the coast is. In practice, it has been chosen such that $h(b) = 22.5$ m (Clarke and Brink, 1985), and such that $h(b)$ is equal to three times the Ekman layer e-folding decay scale δ [19].

In the absence of turbulent stress, (1)–(5) can be reduced to one single equation for P. Let $\zeta = \frac{\partial v}{\partial x} - \frac{\partial u}{\partial y}$ and $\mathcal{D} = \frac{\partial u}{\partial x} + \frac{\partial v}{\partial y}$, respectively, be vorticity and divergence, then it is easy to obtain

$$\zeta_t + f\,\mathcal{D} = 0,$$
$$\mathcal{D}_t - f\zeta = -\frac{1}{\rho_0}\nabla^2 P.$$

But $\mathcal{D} = -\mathcal{W}_z = \frac{\partial}{\partial z}\left(\frac{1}{\rho_0 N^2} P_{zt}\right)$ by the continuity and hydrostatic equations (4) and (5). These yield

$$\left(f^2 + \frac{\partial^2}{\partial t^2}\right)\frac{\partial}{\partial z}\left(\frac{P_{zt}}{N^2}\right) + \nabla^2 P_t = 0. \tag{6}$$

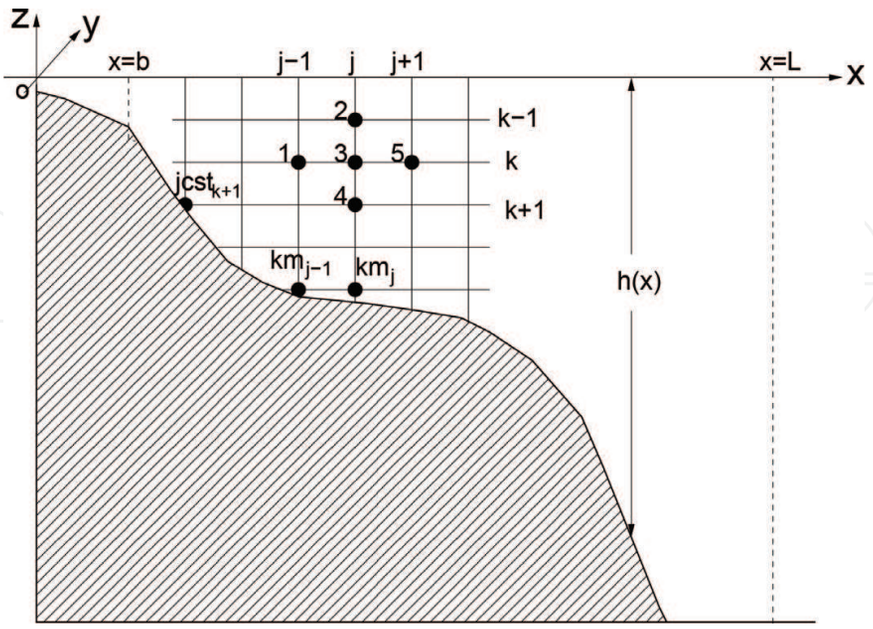


Figure 2. A schematic of the topographic configuration and its discretization (k and j are the indices). The location $x = b$ is pretended to be where the coast lies.

http://dx.doi.org/10.5772/intechopen.80017

In the *"long-wave limit"*

$$\partial^2/\partial t^2 \ll f^2, \qquad \partial^2/\partial y^2 \ll \partial^2/\partial x^2,$$

the equation is simplified to

$$\frac{P_{xxt}}{f^2} + \left(\frac{P_{zt}}{N^2}\right)_z = 0. \tag{7}$$

With the same long-wave assumption, the boundary conditions are (Clarke and Van Gorder [20]):

$$\text{at } x = b, \qquad P_{xt} + \frac{rP_x}{h} + fPy = \frac{f\tau^y}{h} \tag{8}$$

$$\text{at } z = 0, \qquad P_z = 0 \quad (\text{rigid lid}), \quad \text{or} \qquad P_z + \frac{N^2}{g}P = 0 \quad (\text{free surface}) \tag{9}$$

$$\text{at } z = -h, \qquad \frac{f^2 P_{zt}}{N^2} + h_x\left(P_{xt} + fP_y\right) + (rP_x)_x - h_x r P_{xz} = 0, \tag{10}$$

$$\text{as } x \to \infty, \qquad P_x \to 0, \tag{11}$$

where τ^y is the alongshore component of the wind stress, and r is the coefficient of the y-bottom drag in a linear form: $\tau_B^y = \rho_0 r v_B$. Note Eq. (11) is the far field condition; in practice, it may be replaced by another convenient condition ($u_x = 0$ at $x = L$) (see [10]). Eq. (8) is the no-flux condition: $\int_{-h(b)}^{0} u dz = 0$.

Eq. (9) is the boundary condition at $z = 0$ for a rigid-lid or a free surface. In this study, we will adopt the rigid-lid assumption, which implies a nondivergent horizontal flow, and effectively filters out the fast external waves. In the YS/ECS case, there have been strong arguments against using it because the number $\Gamma = \frac{(fL)^2}{gH}$, where L is the width of continental shelf and H the typical depth, is not small (e.g., [11, 15, 18]). Here for the purpose of this monograph, we will focus on the climatic variability of the YS CTWs, which are only associated with slow modes. As such, a rigid lid on top of the ocean makes a more convenient configuration. For discussions on the free surface condition, see, e.g., Brink [19].

Motivated by the form of (7), Clarke and Van Gorder [20] introduced a vector

$$\mathbf{M} = \frac{P_x}{f^2}\mathbf{i} + \frac{P_z}{N^2}\mathbf{k}, \tag{12}$$

and the equation is then simply $\nabla \cdot \mathbf{M}_t = 0$.

2.2. Eigenvalue problem

In order to avoid getting into too much technical details, we only consider the frictionless situation: $r = 0$. For free CTWs, $\tau^y = 0$. We seek a wave solution in the form

$$P(x,y,z;t) = F(x,z)\ \ \phi(y-ct). \tag{13}$$

Substitution of it back into (7) and the boundary conditions (8)–(11) gives

$$\frac{F_{xx}}{f^2} + \left(\frac{F_z}{N^2}\right)_z = 0, \tag{14}$$

$$\text{at } z = 0, \qquad F_z = 0, \tag{15}$$

$$\text{at } x = b, \qquad \frac{c}{f}F_x - F = 0, \tag{16}$$

$$\text{at } z = -h(x), \qquad c\left(h_x F_x + \frac{f^2}{N^2}F_z\right) - fh_x F = 0, \tag{17}$$

$$\text{as } x \to \infty, \qquad F_x \to 0. \tag{18}$$

Note the minus signs in the conditions at $x = b$ and $z = -h(x)$; they are positive in Brink [19] and Clarke [8] because a left-hand coordinate system is adopted therein. In terms of the vector **M** introduced by Clarke and Van Gorder [20]), the solution form is $\mathbf{M} = \mathbf{B}\ \ \phi(y-ct)$, where

$$\mathbf{B} = \frac{F_x}{f^2}\mathbf{i} + \frac{F_z}{N^2}\mathbf{k}. \tag{19}$$

Let the whole domain for the configuration (cf. **Figure 2**) be Ω and denote the boundary that encloses it as $\partial\Omega$. Introduce an inner product space H over Ω. Its inner product $\langle F_m, F_n\rangle_{\mathcal{H}}$ is defined such that, for any $F, G \in H$,

$$\langle F, G_{\mathcal{H}}\rangle = \int_{-h(b)}^{0} FG\Big|_{x=b} dz + \int_{b}^{\infty} h_x FG\Big|_{z=-h(x)} dx. \tag{20}$$

Considering the vanishing far field condition and the rigid-lid surface condition, this is actually an inner product evaluated at the boundary $\partial\Omega$. This is quite different from the inner product space in the usual sense. It is easy to show that $\langle F_m, F_n\rangle_{\mathcal{H}}$ satisfies the needed axioms.

Let $\{F_m\}$ be a set of the eigenfunctions of (14)–(18). Clearly $F_m \in H$ for all integers m; they possess the following important property [7, 8]:

Theorem 2.1 *$\{F_m\}$ forms an orthogonal set in H; that is to say, $\langle F_m, F_n\rangle_{\mathcal{H}} = 0$ if $m \neq n$.*

PROOF. The orthogonality can be proved in different ways. In Clarke and Van Gorder [20], it is easily obtained through manipulating the identity

$$\nabla \cdot (F_n \mathbf{B}_m - F_m \mathbf{B}_n) = 0,$$

which integrated over Ω must also vanish. By Gauss' theorem,

$$\int_{\partial\Omega} \mathbf{n} \cdot (F_n \mathbf{B}_m - F_m \mathbf{B}_n) ds = 0,$$

where ds is the arc length along $\partial\Omega$. With the boundary conditions taken into account, this becomes

$$\left(\frac{1}{c_n} - \frac{1}{c_m}\right)\left[\int_{x=b} F_m F_n ds + \int_{z=-h(x)} h_x \frac{F_m F_n}{\sqrt{1+h_x^2}} ds\right] = 0.$$

For $m \neq n$, this is

$$\int_{x=b} F_m F_n ds + \int_{z=-h(x)} \frac{h_x}{\sqrt{1+h_x^2}} F_m F_n ds = 0,$$

or

$$\int_{-h(b)}^{0} F_m(0,z) F_n(0,z)\ dz + \int_{x=b}^{\infty} F_m(x,-h(x))\ F_n(x,-h(x)) h_x\ dx = 0. \tag{21}$$

Q.E.D.

This theorem states that the eigenvectors are orthogonal in the inner product space H. They can always be normalized by the induced norm $\|F_m\| = \sqrt{\langle F_m, F_m \rangle_{\mathcal{H}}}$, and then form an orthonormal set. [$\|F_m\|$ is shown to be f; see Clarke [8]]. Caution should be used, however, in the normalization, which must be made such that energy is conserved as waves propagate through a slowly varying medium [21].

From the orthogonality condition Wang and Mooers [7] connected CTWs to internal Kelvin waves (flat bottom), shelf waves, and topographic Rossy waves ($b = 0$). They also showed that there exists another orthogonality condition over Ω rather than along $\partial\Omega$; that is:

$$\int_{b}^{\infty} \int_{-h(x)}^{0} \left[\left(\frac{\partial F_n}{\partial x}\right)\left(\frac{\partial F_m}{\partial x}\right) + \frac{1}{N^2}\left(\frac{\partial F_n}{\partial z}\right)\left(\frac{\partial F_m}{\partial z}\right) + \ell^2 F_n F_m\right] dx dz = 0,$$

if $c_n \neq c_m$, where ℓ is the wavenumber in y. But whether this satisfies the inner product axioms is yet to be checked.

In addition to orthogonality, it is also possible to prove that $\{F_m\}$ forms a complete set (see Courant and Hilbert, pp. 424–426). That is to say, the normalized $\{F_m\}$ makes a basis of H.

2.3. Excitation of CTWs

By the forgoing argument, $\{F_n\}$ makes a basis of H. Thus, any function of H, P in particular, can be written as a linear combination of F_n, $n = 1, 2, \ldots$,

$$P = \sum_{n=1}^{\infty} F_n(x,z)\phi_n(y,t). \tag{22}$$

When a forcing τ^y is applied at the boundary, we can then solve for the amplitudes ϕ_n.

Usually, the amplitude equation can be obtained through taking the inner product of F_n with the governing Eq. (7), or $\nabla \cdot \mathbf{M}_t = 0$. In this particular case, it is not this straightforward because the inner product is evaluated along the boundary $\partial\Omega$, rather than in Ω. Besides multiplying F_n with $\nabla \cdot \mathbf{M}_t$, Clarke and Van Gorder [20] considered a duality $P_t\mathbf{B}_n$. They found that

$$\nabla \cdot (F_n\mathbf{M}_t - P_t\mathbf{B}_n) = 0,$$

which of course vanishes if integrated over Ω. By Gauss' theorem,

$$\oint_{\partial\Omega} \mathbf{n} \cdot (F_n\mathbf{M}_t - P_t\mathbf{B}_n)ds = 0.$$

Expanding and taking into account of the boundary conditions, this is eventually reduced to (see Clarke and Van Gorder [20])

$$\int_{-h(b)}^{0} \left[F_n\left(P_y - \frac{P_t}{c_n}\right)\right]_{x=b} dz + \int_{-h(b)}^{0} \left(\frac{F_n r P_x}{fh}\right)_{x=b} dz + \int_b^{\infty} \left[F_n\left(P_y - \frac{P_t}{c_n}\right)\right]_{z=-h(x)} dx$$
$$+ \int_b^{\infty} F_n(x,-h)\frac{d}{dx}\left(\frac{rP_x(x,-h(x))}{f}\right) dx = \left(\int_{-h(b)}^{0} F_n(b,z)\ dz\right)\frac{\tau^y(y,t)}{h(b)}.$$

Substitution of (22) for P, and use of the orthogonality property: $\langle F_m, F_n\rangle_{\mathcal{H}} = 0$ if $m \neq n$, yields

$$-\frac{1}{c_n}\frac{\partial\phi_n}{\partial t} + \frac{\partial\phi_n}{\partial y} + \sum_{m=1}^{\infty} a_{mn}\phi_m = b_n\tau^y(y,t),$$

where

$$b_n = \frac{1}{D_n h(b)}\int_{-h(b)}^{0} F_n(b,z)dz,$$

$$a_{mn} = \frac{1}{D_n}\left[\int_b^{\infty} F_n(x,-h)\frac{1}{f}\frac{d}{dx}(rF_{mx}(x,-h))\ dx + \int_{-h(b)}^{0}\left[\frac{F_n r F_{mx}}{fh}\right]_{x=b} dz\right]$$

$$D_n = \langle F_n, F_n\rangle_{\mathcal{H}} = \|F_n\|^2.$$

In the case, only one mode n is excited, there is no coupling: $\sum_1^{\infty} a_{mn}\phi_m = a_{nn}\phi_n$ (e.g., Battisti and Hickey [22]), the amplitude equation can be solved analytically in terms of characteristic coordinates [19].

$$s = t - \int_y^0 c_n^{-1}dy',$$
$$\xi = y.$$

In this case,

http://dx.doi.org/10.5772/intechopen.80017

$$\phi_n(y,t) = \phi_n\left(0,\ \ t - \int_y^0 c_n^{-1} d\xi\right) \cdot e^{-\int_y^0 a_{nn} d\xi} + \int_y^0 b_n(\xi)\tau^y \left(\xi,\ \ t - \int_y^\xi c_n^{-1} d\xi'\right) \cdot e^{-\int_y^\xi a_{nn} d\xi'}\ \ d\xi,$$

where $y = 0$ signifies the starting point of the calculation. See Brink [19] for details.

Once ϕ is solved, P may be obtained through reconstruction with modes. From (1)–(2), it is easy to obtain $v_{tt} + f^2 v = -\frac{1}{\rho_0} P_{yt} + \frac{f}{\rho_0} P_x$, which in the long-wave limit simply shows the geostrophic balance: $f^2 v = f P_x / \rho_0$. The fields then can be obtained accordingly:

$$u = -\frac{1}{\rho_0 f^2}\left(P_{xt} + f P_y\right),$$
$$v = \frac{1}{\rho_0 f} P_x,$$
$$w = -\frac{P_{zt}}{\rho_0 N^2},$$
$$\rho = -\frac{1}{g} P_z.$$

3. The CTWs off the Subei Bank in the Yellow Sea

3.1. Background fields

We choose a cross-section outside the Subei Bank as shown in **Figure 1**. It is chosen in the middle since in the north the shelf is too shallow, while in the south the Changjiang diluted water complicates the circulation system very much and hence may disguise the wave propagation. The HYCOM data are used to set up the model; they are advantageous in that tides are excluded in the reanalysis fields. The horizontal resolution is 0.1° in longitude, by 0.0702° in latitude, which results in a horizontal spacing of 12 km along the section. In the vertical direction, the levels are at 0, 2, 4, 6, 8, 10, 12, 15, 20, 25, 30, 35, 40, 45, 50, 60, 70, 80 m, respectively. The data are available for 1993 through 2013. After 2013, the vertical resolution is too coarse for our purpose, and hence they are not considered in this study.

The topography along the section is displayed in **Figure 1b**; it is slightly modified to avoid the bumps (the dashed line). The basic buoyancy frequencies differ year by year. They are calculated from the annual mean density anomaly profiles averaged over along the section. Shown in **Figure 1c** is such an example.

3.2. Eigenvalues and eigenmodes

With the background field, we solve the eigenvalue problem. The solution method is referred to the appendix; it is essentially the same as that by Brink [10], Clarke and Gorder [20], and Wilkin and Chapman [23]. Considering the broad shallow shelf, we artificially set the coastline at the isobath $H = 10$ m. By computation, four typical trapped eigenmodes have been identified. For the year of 2000, the celerities are, in order of magnitude, −0.12, −0.19, −0.21, −0.29 m/s;

the corresponding modes will be henceforth refer to as M1, M2, M3, and M4, respectively. Besides, many slower modes such $c = -0.0046$ m/s have also been found, because the model is too coarsely resolved that we do not consider them here. Similarly, a few higher modes, particularly the one with $c = -0.57$ m/s, are evident. But these higher modes are not trapped to the western topography or coast and hence should be discarded. An observation is that all these celerities are negative; that is to say, all the corresponding waves propagate to the south. This is the very important property of CTW: in the Northern Hemisphere, the wave propagates with the coast on the right hand side.

In order to see whether these eigenvalues indeed exist, we examine the time series at two points $A(122.6^oE, 34.825^oN)$ and $B(122.9^oE, 34.035^oN)$ (see **Figure 1**). They are roughly along the isobath $H \approx 64$ m, located ~ 92 km apart. Again, we use the HYCOM reanalysis data to form the time series. Since too many data are missing for the flow field, consider only the density anomaly. The series are from January 01, 1993 through December 31, 2012, with an interval of 1 day.

The dominant modes of the series have periods of 365 and 183 days, respectively; these are the annual and biannual modes (not shown). However, in the weather frequency band, a local peak is also significant. We use the wavelet method to filter out the signal within this band. Choose the series between October 12, 2001 to December 31, 2012 to ensure that they have a length of $4096 = 2^{12}$ steps (a length of power of 2 is required). We use the orthonormalized cubic spline wavelets constructed in Liang and Anderson (2007) to fulfill the filtering. The scale window is chosen to be bounded by periods 2 and 16 days, respectively. This roughly corresponds to the weather frequency band. We then perform a time-delayed correlation analysis with the two band-pass filtered series, written $\rho_A(t)$ and $\rho_B(t)$. Given a delay τ (in days), we then compute the correlation coefficient $\gamma(\tau)$ between $\rho_A(t)$ and $\rho_B(t+\tau)$. (τ should not be too large, in accordance with the weather frequency band requirement.) Suppose that $\gamma(\tau)$ takes its maximum at T, then the phase speed can be estimated to be d/T. Notice that it is not a good idea to compute γ for all the 4096 days, since the CTWs are coastal wind-driven and within the weather frequency band (1 week or 2 weeks or so). Different modes may be excited during different periods. We hence choose to do the correlation analysis every 30 days. The results

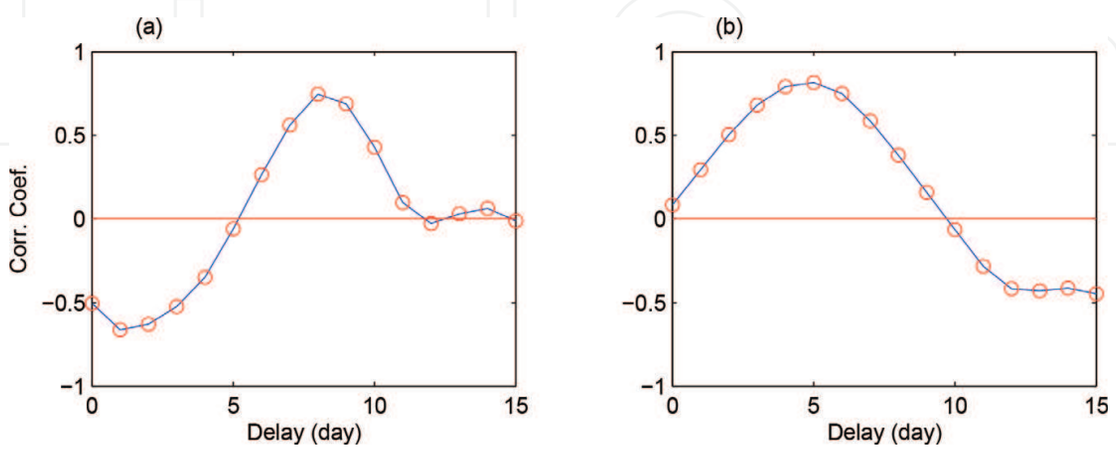


Figure 3. The correlation coefficients between ρ_A and the delayed ρ_B for the periods (a) 12 Aug 2005–2011 Sep 2005 and (b) 04 Feb 2011–2106 Mar 2011. The locations A and B are marked in **Figure 1**.

http://dx.doi.org/10.5772/intechopen.80017

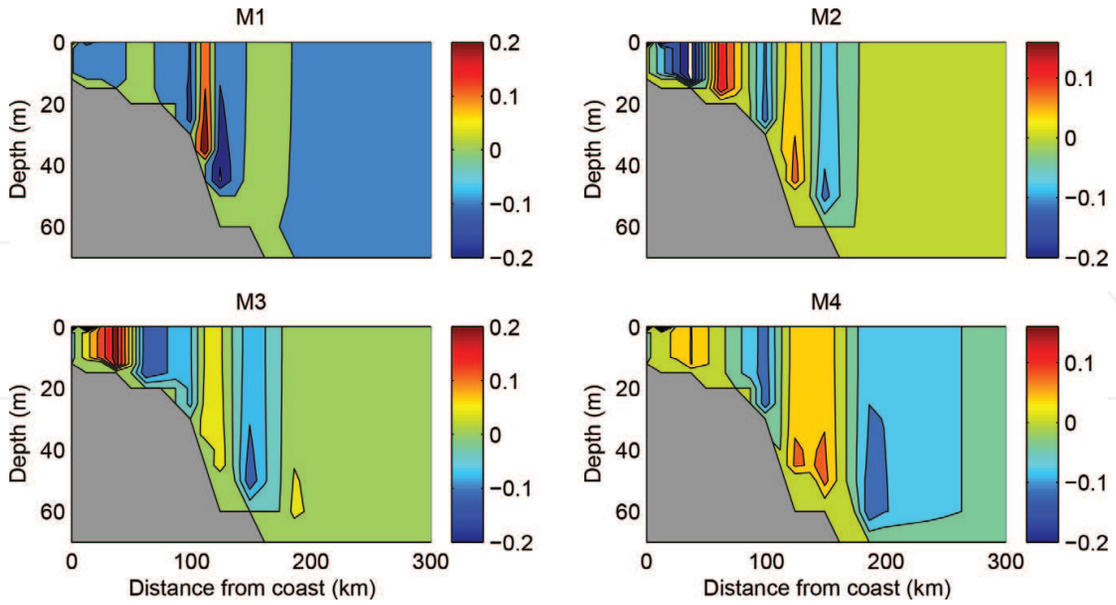


Figure 4. The cross-section structures of the four coastal trapped wave modes M1, M2, M3, and M4, which have celerities of $c = -0.12, -0.19, -0.21, -0.29$ m/s, respectively.

may differ, but the CTW modes consistent with our calculation frequently show up. For example, in **Figure 3a**, the maximum γ takes place at a delay of 8 days for ρ_B, so the modal phase velocity is $92000/(8 \times 24 \times 3600) = 0.13$ m/s. Similarly, in **Figure 3b**, γ takes its maximum at 5 days, which corresponds to a speed of 0.21 m/s. Considering there may be a slight change in magnitude with time (see below), these celerities agree very well with the celerities of M1 ($c = 0.12$) and M3 ($c = 0.21$) in 2000. We actually find many cases with a speed of 0.53, a high mode that have been discarded, and many other slower modes, which we do not consider here. Note the time resolution (1 day) of the series cannot distinguish M2 and M3.

The eigenmodes corresponding to the four celerities are shown in **Figure 4**. From it we see that, the slower the wave, the more topographically trapped the structure. Particularly, in the first subplot, we see a bottom-trapped mode ($c = -0.12$ m/s).

The modal structures for other years are similar, but the propagating speeds differ. In the next section, we will see more details about this.

4. The change in CTW celerities during the past 20 years

The buoyancy frequency profiles change with time, which will inevitably affect the CTW propagating properties. We have computed the eigenvalues for the six identified modes for all the past 20 years. The results are shown in **Figure 5**.

Interestingly, from the figure, all the identified modes seem to have the same evolutionary trend. On the whole, the computed speeds are all on decline (note the negative sign) during the past 20 years. This might be related to global warming, but what makes it puzzling is that, simply

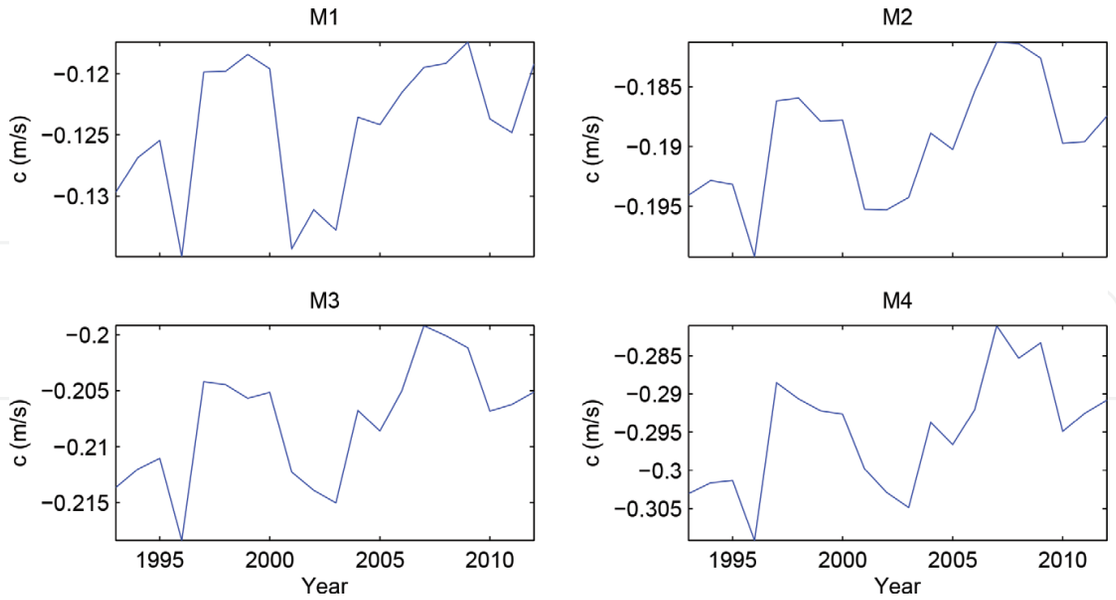


Figure 5. Time variation of the celerities of the four modes M1–M4 as shown in **Figure 4**.

warming the ocean cannot change the CTW wave propagating; rather, it is the alteration of the vertical stratification that may cause the change. For such a shallow sea, it is still unclear how this can be fulfilled. Even though it is related to global warming, it must be through some third mechanism(s). In the Yellow Sea, a conspicuous hydrographic feature is its cold water mass in summer; maybe that functions to mediate the events–we will explore this in future studies.

Another interesting feature of **Figure 5** is the maxima (or minima if magnitude is considered) around 1997 and 2009. This reminds one of El Niño, as around those are the El Niño years; particularly, the 97–98 El Niño is very strong, as shown in **Figure 6**. However, from the figure one may argue that 02–03 is also a moderately strong El Niño year, while in **Figure 5**, the *c*'s reach their respective minima. We hence need to pick more quantity to compare. As shown in **Figure 6**, the La Niña intensity may be such a candidate. Notice that immediately after the 97–98 El Niño, there is a strong La Niña; same happens after the 09–10 one, while after 2003 no La Niña occurs at all. Therefore, it seems that the CTWs are greatly slowed down when a strong El Niño followed by a strong La Niña occurs.

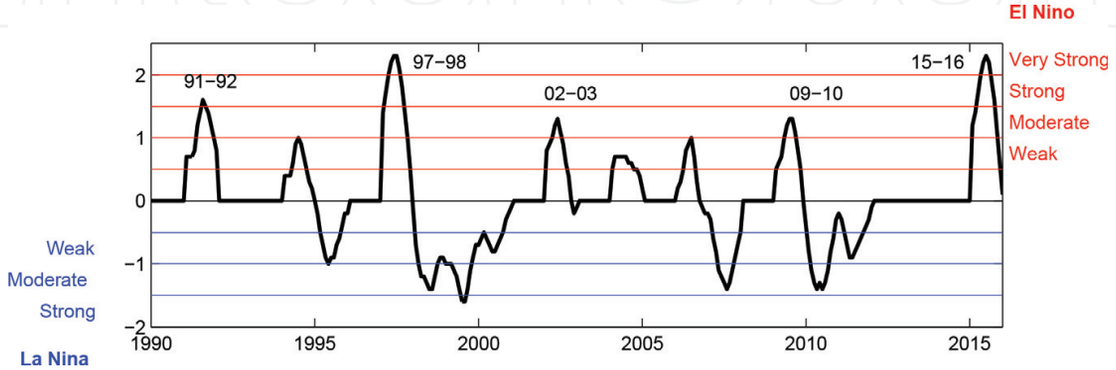


Figure 6. ENSO events and their intensities since 1990. The figure is based on the Oceanic Niño Index; see http://www.cpc.ncep.noaa.gov/products/analysis_monitoring/ensostuff/ensoyears.shtml.

http://dx.doi.org/10.5772/intechopen.80017

We emphasize that we do not claim that ENSO has caused the slow-down of the CTWs. What we have shown is just a remarkable correlation between the wave property change and the ENSO occurrence—In fact, even correlation may not be an appropriate term here. We should have computed the correlation coefficients between the *c*'s and some ENSO index, say, the Oceanic Niño Index as shown in **Figure 6**, but the time resolution of the *c* series are very low; there is only one value per year. We have also tried CTW configurations with monthly mean fields, but the dominating seasonal cycle completely disguises the signal, which just worsens the situation.

5. Concluding remarks

Coastal trapped waves (CTW), which flourished during 60–80s, thanks to the efforts from investigators such as Allen [6], Wang and Mooers [7], Clarke [8], Huthnance [9], Mysak [24], Brink [19], Chapman [25], among many others, play an important role in the processes of coastal and continental oceans (cf. [10]). However, this important topic seems to be missing in the heated debate in recent years on coastal environmental change and protection. In this chapter, we have given a brief but self-contained introduction of the CTW theory, in the hope of gaining renewed interest in this field. The nice properties such as the mutual orthogonality between the eigenmodes make this class of waves not just important in practice, but also theoretically appealing. For reference, a numerical scheme is supplied in the appendix to solve the resulting eigenvalue problem.

As a demonstration, we have conducted a preliminary study of the CTWs for a section across Subei Bank in the Yellow Sea, a region where traditionally the role of CTWs has been overlooked due to its shallow depth. Considering the scope of this monograph, we have particularly focused on the slow wave modes and their variabilities during the past decades. Interestingly, all the identified prominent modes, including a bottom-intensified one, seem to be slowing down during the past 20 years. Particularly, it seems that they are greatly slowed down during the events when a strong El Niño is followed by a strong La Niña, such as the 97–98 and 09–10 El Niño events.

However, caution should be used in interpreting these results. Apart from the poor time resolution (one value per year), the obtained *c*-series are not long enough for climate variability studies. It would be better if the data can be extended so that decadal variability can be examined; particularly one would like to see how they behave during the two super El Niño years: 1982–1983 and 2015–2016 (currently data are not available). We will investigate this in future studies.

Acknowledgements

Section 2 and Appendix are extracted from an unpublished technique report (Liang [26]) by the author in the former Harvard Ocean Group, which was prepared for the project AOSN-II then (cf. [27]). Thanks are due to Kenneth Brink for the help in drafting that report. The HYCOM group is acknowledged for proving the reanalysis data. Yineng Rong prepared the

background field of the cross-section and the point series for analysis and drew **Figure 1**. This study was partially supported by the 2015 Jiangsu Program for Innovation Research and Entrepreneurship Groups, by the National Program on Global Change and Air-Sea Interaction (GASI-IPOVAI-06), and the National Science Foundation of China under Grant 41,276,032 [28–30].

A. A numerical solver for coastal-trapped waves

The x–z domain is discretized into a mesh grid, as sketched in **Figure 2**. The spacings Δx and Δz may vary with the respective indices j and k. We use j, instead of i, to indicate the x index,

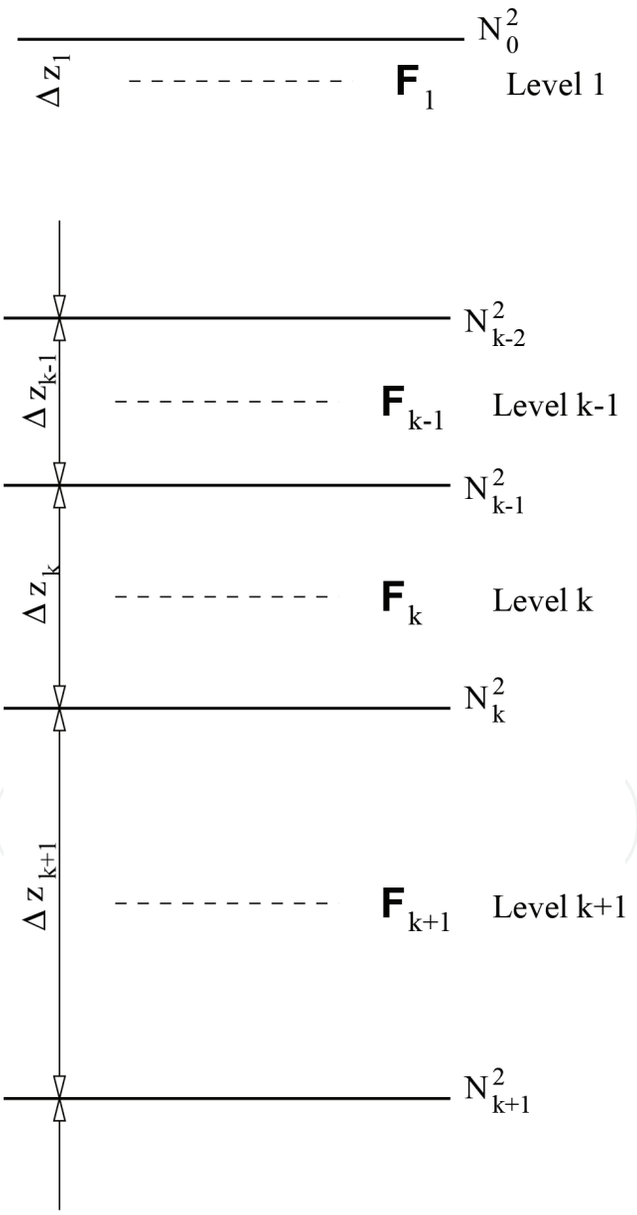


Figure 7. Discretization in the z direction.

in order not to confuse with the complex number $\sqrt{-1}$. In the grid, the eigenfunction F is defined at integer points k, while the buoyancy frequency N^2 is at half integer points (**Figure 7**).

For j, let j_b and j_m be the boundary limits, which correspond to $x = b$ and $x = L$ (L some large number). Note for each horizontal level k, the limits for j should be $j_{cst}(k)$ and j_m, with j_{cst} dependent on k. Similarly denote the bottom index as k_m, then k runs from 1 to k_m, and the rigid-lid and bottom correspond to $k = \frac{1}{2}$ and $k = k_m + \frac{1}{2}$, respectively. The limit $k_m = k_m(j)$ is a function j, which is determined by the function $h(x)$.

Let

$$\delta(x) = \begin{cases} 1, & x = 0; \\ 0, & x \neq 0, \end{cases}$$

and

$$\begin{aligned} \delta^{sea} &\equiv \delta\big(j - j_\infty\big); & c^{sea} &\equiv 1 - \delta^{sea} \\ \delta^{cst} &\equiv \delta\big(j - j_{cst}(k)\big); & c^{cst} &\equiv 1 - \delta^{cst} \\ \delta^{top} &\equiv \delta(k - 1); & c^{top} &\equiv 1 - \delta^{top} \\ \delta^{bot} &\equiv \delta(k - k_m(j)); & c^{bot} &\equiv 1 - \delta^{bot}. \end{aligned}$$

Further define

$$\begin{aligned} \Delta_x^+ &\equiv \frac{\Delta x_{j+1} + \Delta x_j}{2}, & \Delta_z^+ &\equiv \frac{\Delta z_{k+1} + \Delta z_k}{2}, \\ \Delta_x^- &\equiv \frac{\Delta x_{j-1} + \Delta x_j}{2}, & \Delta_z^- &\equiv \frac{\Delta z_{k-1} + \Delta z_k}{2}, \\ \gamma_x^+ &\equiv \frac{\Delta x_j - \Delta x_{j+1}}{2\big(\Delta_x^+ + \Delta_x^-\big)}, & \gamma_z^+ &\equiv \frac{\Delta z_k - \Delta z_{k+1}}{2\big(\Delta_z^+ + \Delta_z^-\big)}, \\ \gamma_x^- &\equiv \frac{\Delta x_{j-1} - \Delta x_j}{2\big(\Delta_x^+ + \Delta_x^-\big)}, & \gamma_z^- &\equiv \frac{\Delta z_{k-1} - \Delta z_k}{2\big(\Delta_z^+ + \Delta_z^-\big)}. \end{aligned}$$

Then

$$\frac{\partial^2 F}{\partial x^2} = \frac{1}{\Delta x_j} \cdot \left\{ c^{sea} \cdot \left[\frac{F_{j+1,k} - F_{j,k}}{\Delta_x^+} + \gamma_x^+ c^{cst} \left(\frac{F_{j+1,k} - F_{j,k}}{\Delta_x^+} - \frac{F_{j,k} - F_{j-1,k}}{\Delta_x^-} \right) \right] + \delta^{sea} \cdot \left(\frac{\partial F}{\partial x} \right) \Big|_{(\infty,k)} \right.$$

$$\left. - c^{cst} \cdot \left[\frac{F_{j,k} - F_{j-1,k}}{\Delta_x^-} + \gamma_x^- c^{sea} \left(\frac{F_{j+1,k} - F_{j,k}}{\Delta_x^+} - \frac{F_{j,k} - F_{j-1,k}}{\Delta_x^-} \right) \right] - \delta^{cst} \cdot \left(\frac{\partial F}{\partial x} \right) \Big|_{(j_{cst}(k),k)} \right\},$$

and

$$f^2\left(\frac{F_z}{N^2}\right)_z = \frac{f^2}{\Delta z_k}\cdot\left\{\frac{c^{top}}{N^2_{k-1/2}}\cdot\left[\frac{F_{j,k-1}-F_{j,k}}{\Delta_z^-}+\gamma_z^- c^{bot}\left(\frac{F_{j,k-1}-F_{j,k}}{\Delta_z^-}-\frac{F_{j,k}-F_{j,k+1}}{\Delta_z^+}\right)\right]\right.$$
$$+\frac{\delta^{top}}{N^2_{k-1/2}}\cdot\left(\frac{\partial F}{\partial z}\right)\Big|_{(j,1)}-\frac{c^{bot}}{N^2_{k+1/2}}\cdot\left[\frac{F_{j,k}-F_{j,k+1}}{\Delta_z^+}+\gamma_z^+ c^{top}\left(\frac{F_{j,k-1}-F_{j,k}}{\Delta_z^-}-\frac{F_{j,k}-F_{j,k+1}}{\Delta_z^+}\right)\right]$$
$$\left.\times-\frac{\delta^{bot}}{N^2_{k+1/2}}\cdot\left(\frac{\partial F}{\partial z}\right)\Big|_{(j,k_m(j)}\right\},$$

where the boundary conditions are

$$\left(\frac{\partial F}{\partial x}\right)\Big|_{(\infty,k)}=0,$$
$$\left(\frac{\partial F}{\partial x}\right)\Big|_{(j_{cst}(k),k)}=\frac{f}{c}F_{j_{cst}(k),k},$$
$$\left(\frac{\partial F}{\partial z}\right)\Big|_{(j,1)}=0,$$
$$\left(\frac{\partial F}{\partial z}\right)\Big|_{(j,k_m(j))}=0.$$

Remarks

- Note here the bottom boundary condition is no longer

$$c\left(h_x F_x+\frac{f^2}{N^2}F_z\right)-fh_x F=0,\qquad \text{at } z=-h(x) \tag{23}$$

as shown before. Because we adopt a staircase-like topography in our discretized domain, (23) is replaced by a horizontal wall condition and a flat-bottom condition.

- In the equation, γ_x^+, γ_x^-, γ_z^+, and γ_z^- have been multiplied respectively by c^{cst}, c^{sea}, c^{bot}, and c^{top} to handle those points near the boundary. In this case, the discretization at these points have only precision of order 1 if the mesh is not uniform.

With the above F_{xx} and F_{zz}, the governing equation

$$\frac{F_{xx}}{f^2}+\left(\frac{F_z}{N^2}\right)_z=0$$

is discretized. Collect the coefficients of $F_{j-1,k}$, $F_{j,k-1}$, $F_{j,k}$, $F_{j,k+1}$, and $F_{j+1,k}$, as correspond to the points 1, 2, 3, 4, and 5 in **Figure 2**. They are:

$$F_{j-1,k}:\frac{1}{\Delta x_j}\frac{1}{\Delta_x^-}\left\{\gamma_x^+ c^{cst}c^{sea}-c^{cst}\left(-1+\gamma_x^- c^{sea}\right)\right\}\equiv a_1(j,k), \tag{24}$$

$$F_{j,k-1}:\frac{f_0^2}{\Delta z_k}\frac{1}{\Delta_z^-}\left\{\frac{c^{top}}{N^2_{k-1/2}}\left(1+\gamma_z^- c^{bot}\right)-\frac{c^{bot}}{N^2_{k+1/2}}\gamma_z^+ c^{top}\right\}\equiv a_2(j,k), \tag{25}$$

http://dx.doi.org/10.5772/intechopen.80017

$$F_{j,k+1}:\frac{f_0^2}{\Delta z_k}\frac{1}{\Delta_z^+}\left\{\frac{c^{top}}{N_{k-1/2}^2}\gamma_z^- c^{bot}-\frac{c^{bot}}{N_{k+1/2}^2}\left(-1+\gamma_z^+ c^{top}\right)\right\}\equiv a_4(j,k), \tag{26}$$

$$F_{j+1,k}:\frac{1}{\Delta x_j}\frac{1}{\Delta_x^+}\left\{c^{sea}\left(1+\gamma_x^+ c^{cst}\right)-\gamma_x^- c^{cst}c^{sea}\right\}\equiv a_5(j,k), \tag{27}$$

$$F_{j,k}:a_3-\eta_{j,k}\cdot\frac{1}{c}, \tag{28}$$

where

$$\begin{aligned}a_3(j,k)=\frac{1}{\Delta x_j}\Bigg\{&c^{sea}\cdot\left[-\frac{1}{\Delta_x^+}+\gamma_x^+ c^{cst}\left(-\frac{1}{\Delta_x^+}-\frac{1}{\Delta_x^-}\right)\right]\\&-c^{cst}\cdot\left[\frac{1}{\Delta_x^-}+\gamma_x^- c^{sea}\left(-\frac{1}{\Delta_x^+}-\frac{1}{\Delta_x^-}\right)\right]\Bigg\}\\&+\frac{f^2}{\Delta z_k}\Bigg\{\frac{c^{top}}{N_{k-1/2}^2}\cdot\left[\frac{1}{\Delta_z^-}+\gamma_z^- c^{bot}\left(-\frac{1}{\Delta_z^-}-\frac{1}{\Delta_z^+}\right)\right]\\&-\frac{c^{bot}}{N_{k+1/2}^2}\cdot\left[\frac{1}{\Delta_z^+}+\gamma_z^+ c^{top}\left(-\frac{1}{\Delta_z^-}-\frac{1}{\Delta_z^+}\right)\right]\Bigg\},\end{aligned}$$

and

$$\eta_{j,k}=\frac{1}{\Delta x_j}\delta^{cst}f. \tag{29}$$

We would like to make (24)–(28) into a matrix with eigen value $\frac{1}{c}$. But here the problem is unusual, since $\frac{1}{c}$ take values only on boundaries [see the η in (28)], reflecting the fact that the inner product is defined along boundaries. To make it valid throughout the domain, let ε be some small number reflecting the machine precision, say, 10^{-7}, and define a new η such that

$$\eta_{j,k}=\varepsilon\cdot\max_{l=1}^{5}\{|a_l|\}\qquad\text{if }\ \eta_{j,k}=0.$$

Now, the equation with the new η should be the same as the old one up to the machine precision. Write

$$\tilde{a}_l=\frac{a_l}{\eta},\quad l=1,2,\ldots,5. \tag{30}$$

The discretized equation is then

$$\tilde{a}_5 F_{j+1,k} + \tilde{a}_4 F_{j,k+1} + \left(\tilde{a}_3 - \frac{1}{c}\right) F_{j,k} + \tilde{a}_2 F_{j,k-1} + \tilde{a}_1 F_{j-1,k} = 0. \tag{31}$$

And the whole problem is now translated into finding the eigenvalue $\frac{1}{c}$ for a pentadiagonal matrix A, with entries along the five diagonal being $\tilde{a}_i$, $i = 1, 2, 3, 4, 5$.

Author details

X. San Liang

Address all correspondence to: x.san.liang@gmail.com

Center for Ocean-Atmosphere Dynamical Studies, Nanjing Institute of Meteorology, Nanjing, P. R. China

References

[1] Huthnance JM. Circulation, exchange and water masses at the ocean margin: The role of physical processes at the shelf edge. Progress in Oceanography. 1995;**35**:353-431

[2] Hamon BV. The spectra of mean sea level at Sydney Coff's harbour and Lord Howe Island. Journal of Geophysical Research. 1962;**67**:5147-5155

[3] Robinson AR. Continental shelf waves and the response of sea level to weather systems. Journal of Geophysical Research. 1964;**69**:367-368

[4] Mysak LA. On the theory of continental shelf waves. Journal of Marine Research. 1967;**25**: 205-227

[5] Brink KH. The coastal Robinson. Dynamics of Atmospheres and Oceans. 2011;**52**(1–2):4

[6] Allen JS. Coastal trapped waves in a stratified ocean. Journal of Physical Oceanography. 1975;**5**:300-325

[7] Wang D-P, Mooers CNK. Coastal-trapped waves in a continuously stratified ocean. Journal of Physical Oceanography. 1976;**6**:853-863

[8] Clarke AJ. Observational and numerical evidence for wind-forced coastal trapped long waves. Journal of Physical Oceanography. 1977;**7**:231-247

[9] Huthnance JM. On coastal trapped waves: Analysis and numerical calculation by inverse iteration. Journal of Physical Oceanography. 1978;**8**:74-92

[10] Chapman DC. Application of wind-forced, long, coastal-trapped wave theory along the California coast. Journal of Geophysical Research. 1987;**92**:1798-1816

[11] Yin L, Qiao F, Zheng Q. Coastal-trapped waves in the East China Sea observed by a mooring array in winter 2006. Journal of Physical Oceanography. 2014;**44**:576-590

[12] Feng S. A model of dissipative trapped-waves on a uniformly sloping shelf of finite width (in Chinese). Chinese Journal of Oceanology and Limnology. 1981;**12**:1-8

[13] Liu Q, Qin Z. Instability of barotropic coastal trapped waves (in Chinese). Chinese Journal of Oceanology and Limnology. 1990;**21**:301-310

[14] Kong X, Yin X, Li F. Continental shelf waves in the East China Sea and its impact to Kuroshio (in Chinese). Acta Oceanologica Sinica. 1992;**14**:8-14

[15] Chen D, Su J. Continental shelf waves study along China coast (in Chinese). Acta Oceanologica Sinica. 1987;**9**:1-15

[16] Zheng Q, Zhu B, Li J, Sun Z, Xu Y, Hu J. Growth and dissipation of typhoon-forced solitary continental shelf waves in the northern South China Sea. Climate Dynamics. 2014;**45**:853-865

[17] Wang J, Yuan Y, Pan Z. Numerical studies and analysis about continental shelf waves (in Chinese). Acta Oceanologica Sinica. 1988;**10**:666-677

[18] Hsueh Y, Pang I-C. Coastally trapped long waves in the Yellow Sea. Journal of Physical Oceanography. 1989;**19**:612-625

[19] Brink KH. A comparison of long coastal trapped wave theory with observations off Peru. Journal of Physical Oceanography. 1982;**12**:897-913

[20] Clarke A, van Gorder S. A method for estimating wind-driven frictional, time-dependent, and stratified shelf and slope water flow. Journal of Physical Oceanography. 1986;**16**:1013-1028

[21] Brink. Coastal-trapped waves and wind-driven currents over the continental shelf. Annual Review of Fluid Mechanics. 1991;**23**:389-412

[22] Battisiti DS, Hickey BM. Application of remote wind-forced coastal trapped wave theory to the Oregon and Washington coasts. Journal of Physical Oceanography. 1984;**14**:887-903

[23] Wilkin JL, Chapman DC. Scattering of continental shelf waves at a discontinuity in shelf width. Journal of Physical Oceanography. 1987;**17**:713-724

[24] Mysak LA. Recent advances in shelf wave dynamics. Reviews of Geophysics. 1980;**18**:211-241

[25] Clarke AJ, Brink KH. The response of stratified, frictional flow of shelf and slope waters to fluctuating large-scale low-frequency wind forcing. Journal of Physical Oceanography. 1985;**15**:439-453

[26] Liang XS, Anderson DGM. Multiscale window transform. SIAM Journal of Multiscale Modeling and Simulation. 2007;**6**:437-467

[27] Liang XS, Robinson AR. Multiscale processes and nonlinear dynamics of the circulation and upwelling events off Monterey Bay. Journal of Physical Oceanography. 2009;**39**:290-313

[28] Brink KH. Energy conservation in coastal-trapped wave calculations. Journal of Physical Oceanography. 1989;**19**:1011-1016

[29] Chapman DC, Lentz SJ, Brink KH. A comparison of empirical and dynamical hindcasts of low-frequency, wind-driven motions over a continental shelf. Journal of Geophysical Research. 1988;**93**:12409-12422

[30] Liang XS. A Solver for Coastal-Trapped Waves. Cambridge, MA: Technical Report, Harvard Ocean Group, Harvard University; 2004. p. 14

IntechOpen

IntechOpen